ORIGINAL ARTICLE

Annals of Nuclear Medicine Vol. 13, No. 5, 331–336, 1999

Effects of scatter correction on regional distribution of cerebral blood flow using I-123-IMP and SPECT

Hiroshi Ito, Hidehiro Iida, Toshibumi Kinoshita, Jun Hatazawa, Toshio Okudera and Kazuo Uemura

Department of Radiology and Nuclear Medicine, Akita Research Institute of Brain and Blood Vessels

The transmission dependent convolution subtraction method which is one of the methods for scatter correction of SPECT was applied to the assessment of CBF using SPECT and I-123-IMP. The effects of scatter correction on regional distribution of CBF were evaluated on a pixel by pixel basis by means of an anatomic standardization technique. SPECT scan was performed on six healthy men. Image reconstruction was carried out with and without the scatter correction. All reconstructed images were globally normalized for the radioactivity of each pixel, and transformed into a standard brain anatomy. After anatomic standardization, the average SPECT images were calculated for scatter corrected and uncorrected groups, and these groups were compared on pixel by pixel basis. In the scatter uncorrected group, a significant overestimation of CBF was observed in the deep cerebral white matter, pons, thalamus, putamen, hippocampal region and cingulate gyrus as compared with scatter corrected group. A significant underestimation was observed in all neocortical regions, especially in the occipital and parietal lobes, and the cerebellar cortex. The regional distribution of CBF obtained by scatter corrected SPECT was similar to that obtained by O-15 water PET. The scatter correction is needed for the assessment of CBF using SPECT.

Key words: scatter correction, SPECT, I-123-IMP, anatomic standardization

INTRODUCTION

Iodine-123 labeled N-isopropyl-p-iodoamphetamine (^{123}I-IMP) is used as a cerebral blood flow (CBF) tracer in single photon emission computed tomography (SPECT),[1,2] and a simple method for regional CBF measurement with ^{123}I-IMP has been developed, which requires one SPECT scan and one point blood sampling.[3–5] But scatter hampers the quantitative assessment of regional CBF with SPECT, causing systematic underestimation in gray matter and systematic overestimation in white matter, reducing contrast in the reconstructed images.[6]

To reduce the effects of scatter, several methods for scatter correction of SPECT have been proposed.[7–14] The transmission dependent convolution subtraction (TDCS) method is one of the methods which accurately corrects for the scatter in the emission projection by using an empirically determined scatter function and the transmission data.[11,14] Previously we applied the TDCS method to the quantitative assessment of regional CBF with SPECT and ^{123}I-IMP, and it has been shown that use of the TDCS method could improve the contrast between gray and white matter, and reveal CBF values identical to those obtained by positron emission tomography (PET) with ^{15}O labeled water ($H_2{}^{15}O$).[6] In this study, region-of-interest analyses which introduced limitations to the sensitivity of the imaging approaches was used to determine significant CBF changes.

Fox et al. have reported that intersubject averaging of PET images, a technique requiring transformation of brain images of individual subjects into a standard brain shape and size in three-dimensions (*anatomic standardization*), gives enhanced detection of focal brain responses.[15] This anatomic standardization technique permits group comparisons,[16] e.g., scatter corrected vs.

Received April 21, 1999, revision accepted July 15, 1999.

For reprint contact: Hiroshi Ito, M.D., Department of Radiology and Nuclear Medicine, Akita Research Institute of Brain and Blood Vessels, 6–10 Senshu-kubota-machi, Akita 010–0874, JAPAN.

E-mail: hito@akita-noken.go.jp

uncorrected SPECT image, on a pixel-by-pixel basis. Minoshima et al.[17–20] have developed a method for anatomic standardization, and it has been used for group comparisons with PET.[21] Their system transforms the brain anatomical structures of subjects into a standard anatomical format by using linear and nonlinear parameters.

In the present study, the effects of scatter on regional distribution of CBF were evaluated in detail by using this anatomic standardization technique. The TDCS method was applied for scatter correction in ^{123}I-IMP SPECT. The effects of scatter correction on regional distribution of CBF were investigated by comparing the scatter corrected and uncorrected SPECT images on a pixel-by-pixel basis. This study is based on our previous work.[6]

METHODS

Subjects

The study was approved by the Ethics Committees of Akita Research Institute of Brain and Blood Vessels. Six healthy men (22–26 years) were recruited and gave written informed consent. The subjects were healthy according to their medical history, physical examination, blood screening analysis, and magnetic resonance imaging (MRI) of the brain. Three were nonsmokers and the other three were smokers. In each subject, SPECT and PET measurements were performed on the same day.

SPECT procedure

The SPECT scanner used was GCA-7200 (Toshiba Corp., Tokyo, Japan), a dual-head rotating gamma camera fitted with 400 mm focal length, low energy, high resolution, symmetric fan beam collimators. The radius of rotation was set at 132 mm in all studies, resulting in a reconstructed field-of-view of 22 cm diameter. The energy window was selected was 159 keV with 20% width.

After a blank scan for 15 min, the transmission scan was performed for 15 min using one head and a 25 cm long ^{99m}Tc rod source (74 MBq) which was placed at the focus of the collimator. A SPECT scan was initiated at 20 min after intravenous infusion of 111–222 MBq ^{123}I-IMP over 1 min. The SPECT scan protocol consisted of forty 30 second scans with 360° continuous rotation of the camera. The projection data were summed and used for all further analyses.

Image reconstruction

The projection data obtained with the symmetric fan beam collimator were first changed into parallel projections. Image reconstruction was carried out by the ordered-subset expectation maximization (OSEM) algorithm.[22] The reconstructed in plane resolution was approximately 10 mm full width at half maximum (FWHM). The image matrix size was 64 × 64. The attenuation correction was made by two approaches. The first was to use the μ-maps derived from the transmission scan. The second was to use the uniform μ-values of 0.166 cm^{-1} and 0.090 cm^{-1} in the head contour defined on the reconstructed transmission images using edge detection. For the scatter correction by the TDCS method, the μ-map derived from the transmission scan and uniform μ-map of 0.166 cm^{-1} which was the mean μ-value inside the head contour in the six subjects were used. For the attenuation correction without scatter correction, a uniform μ-map of 0.090 cm^{-1} was used which provided relatively homogeneous distribution of CBF throughout the brain and was routinely used. Details of image reconstruction are given in the literature.[6] Finally, three kinds of SPECT images were reconstructed: no scatter corrected with a uniform μ-value of 0.090 cm^{-1} (NoSC); scatter corrected with a uniform μ-value of 0.166 cm^{-1} (SC-constant μ); and scatter corrected with the μ-map derived from the transmission scan (SC-TCT μ).

Scatter correction

Scatter in the measured emission projection data was corrected by the transmission dependent convolution subtraction (TDCS) method,[11] as described in our previous article.[6] This technique is essentially based on the convolution subtraction technique,[7] but estimates the scatter projection by using an empirically determined scatter function and the scatter fraction calculated from the transmission data. Two major modifications were performed when compared with the original TDCS method. First, the scatter fraction curve was derived as an intermediate of the two experimentally determined scatter fraction curves obtained for plane and uniform source distributions.[14] Second, a constant offset was added to the scatter fraction, so as to account for the septal penetration and scatter in the collimator/detector of the 2% abundance 530 keV emission of ^{123}I producing apparent scatter outside the head.

PET procedure

The PET system used was Headtome V dual PET (Shimadzu Corp., Kyoto, Japan) which provides 47 sections with a center to center distance of 3.125 mm.[23] The intrinsic spatial resolution was 4.0 mm in plane and 4.3 mm FWHM axially. With a Butterworth filter, the reconstructed in plane resolution was approximately 8 mm FWHM.

After transmission scan for attenuation correction, a 180 sec scan was performed after continuous intravenous infusion of $H_2{}^{15}O$ for 2 min. The arterial input function was obtained from the left ventricular time-activity curve that was obtained with the PET camera for the heart according to a validated procedure.[24,25] The CBF images were calculated by the autoradiographic method.[26,27]

Anatomic standardization

All reconstructed SPECT and PET images were globally normalized to 1000 counts/pixel for the radioactivity of

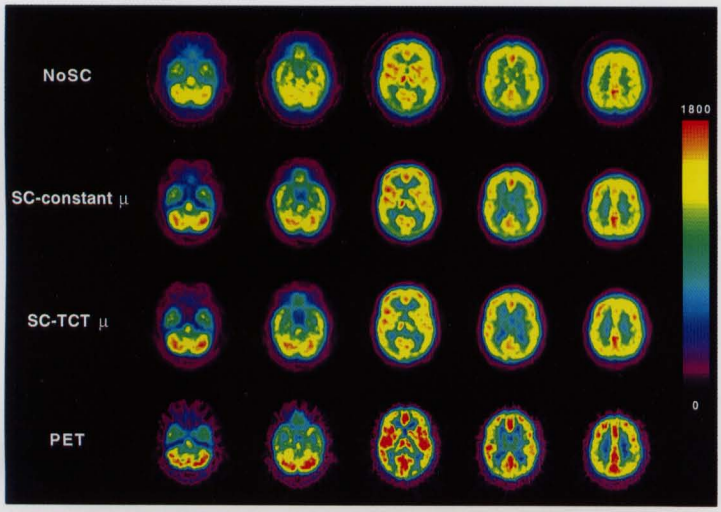

Fig. 1

Fig. 1 The average SPECT images of no scatter correction with the uniform μ-value of 0.090 cm^{-1} (NoSC), scatter correction with the uniform μ-value of 0.166 cm^{-1} (SC-constant μ) and scatter correction with the μ-map derived from the transmission scan (SC-TCT μ), and the average PET image. The pixel values are globally normalized to 1000 counts/pixel. Scale maximum and minimum values are 1800 and 0, respectively.

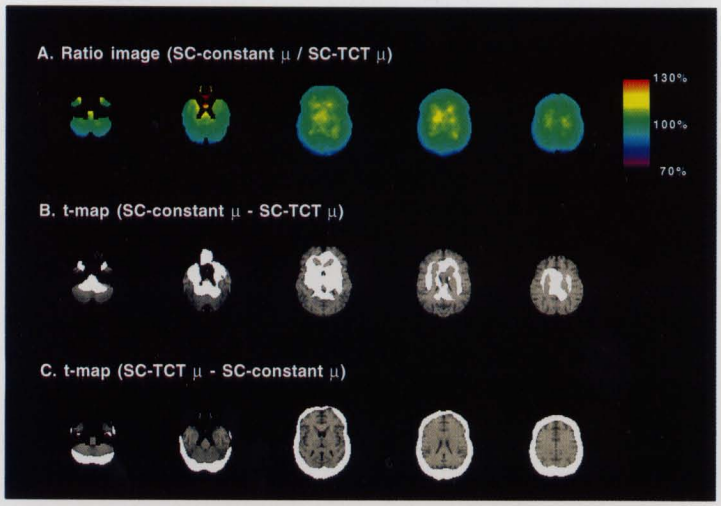

Fig. 2

Fig. 2 The ratio (%) image of SC-constant μ to SC-TCT μ (A) and the t-maps of SC-constant μ minus SC-TCT μ (B) and SC-TCT μ minus SC-constant μ (C). For the t-maps, the areas with positive t-value corresponding to the significance level of $p < 0.01$ are illustrated with white area on the MRI of standard brain. Each slice corresponds to the average SPECT and PET images shown in Figure 1.

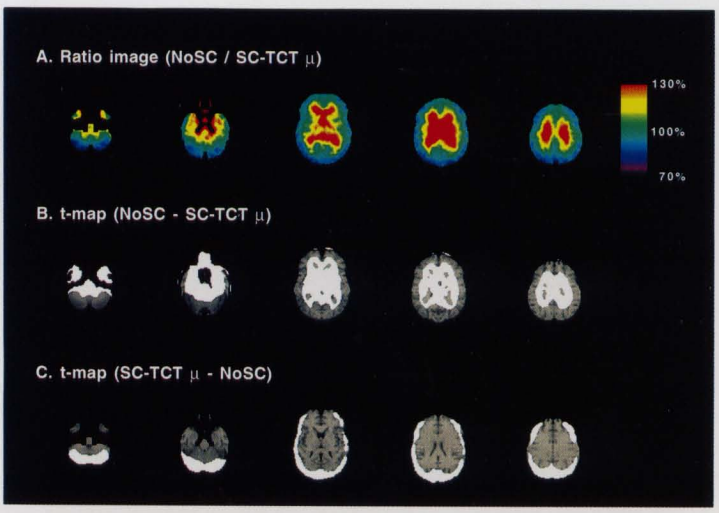

Fig. 3

Fig. 3 The ratio (%) image of NoSC to SC-TCT μ (A) and the t-maps of NoSC minus SC-TCT μ (B) and SC-TCT μ minus NoSC (C). For the t-maps, the areas with t-value corresponding to the significance level of $p < 0.01$ are illustrated with white area on the MRI of standard brain. Each slice corresponds to the average SPECT and PET images shown in Figure 1.

each pixel, and transformed into the standard brain size and shape by linear and nonlinear parameters by using the system for anatomic standardization developed by Minoshima et al.[17–20] After the anatomic standardization procedure, all subjects' SPECT and PET images had the same anatomic brain format. Then the average images of the sample for each group, i.e., scatter corrected SPECT (SC-constant μ, SC-TCT μ), uncorrected SPECT (NoSC) and PET, were calculated and compared on a pixel-by-pixel basis.

From the anatomically standardized SPECT images, descriptive three-dimensional t-maps (paired t-test) of SC-constant μ minus SC-TCT μ and NoSC minus SC-TCT μ were calculated. In the t-maps, the areas with significance level of $p < 0.01$ adjusted for multiple comparison on a pixel-by-pixel basis was considered statistically significant.

RESULTS

The average SPECT images of no scatter correction with the uniform μ-map of 0.090 cm^{-1} (NoSC), scatter correction with the uniform μ-map of 0.166 cm^{-1} (SC-constant μ) and scatter correction with the μ-map derived from the transmission scan (SC-TCT μ) are shown in Figure 1, referring to the average PET image. The regional distribution of the SC-constant μ was in good agreement with that of the SC-TCT μ. The contrast between gray and white matter was higher in the scatter corrected SPECT images (SC-constant μ and SC-TCT μ) than in the no scatter corrected SPECT image (NoSC). The regional distribution of scatter corrected SPECT images (SC-constant μ and SC-TCT μ) was similar to that of PET.

The ratio image of SC-constant μ to SC-TCT μ is shown as a percentage in Figure 2 (A). The t-maps of SC-constant μ minus SC-TCT μ and SC-TCT μ minus SC-constant μ are also shown (B, C). The ratio of SC-constant μ to SC-TCT μ was uniformly around 100%, but an underestimation of CBF of 1–13% for the SC-constant μ as compared with the SC-TCT μ was observed in all neocortical regions, especially in the occipital and parietal lobes. An underestimation of 1–12% was also observed in the cerebellar cortex. On the other hand, an overestimation of CBF of 3–10% for the SC-constant μ as compared with the SC-TCT μ was observed in the deep cerebral white matter and of 5–16% in the pons. In the thalamus, putamen, hippocampal region and cingulate gyrus, the CBF for the SC-constant μ was also overestimated by 1–10% compared to that for the SC-TCT μ. These underestimation and overestimation were significant ($p < 0.01$).

The ratio image of NoSC to SC-TCT μ is shown as a percentage in Figure 3 (A). The t-maps of NoSC minus SC-TCT μ and SC-TCT μ minus NoSC are also shown (B, C). An underestimation of CBF of 1–13% for the NoSC as compared with the SC-TCT μ was observed in all neocortical regions, especially in the occipital and parietal lobes. An underestimation of 3–19% was also observed in the cerebellar cortex. On the other hand, an overestimation of CBF of 15–49% for the NoSC as compared with the SC-TCT μ was observed in the deep cerebral white matter. Overestimations of 9–25%, 12–35%, 2–27%, 12–39% and 1–31% were also observed in the pons, thalamus, putamen, hippocampal region and cingulate gyrus, respectively. These underestimation and overestimation were significant ($p < 0.01$).

DISCUSSION

We have reported that scatter correction with the TDCS method improved the contrast between gray and white matter, and revealed identical CBF values as compared with PET.[6] It has also been shown that the uniform μ-map in the head contour which does not require the transmission scan could be used for attenuation and scatter correction by means of the TDCS method. In the present study the effects of scatter on regional distribution of CBF were evaluated in more detail on a pixel-by-pixel basis by using the anatomic standardization technique.

Regional differences of attenuation coefficient

The regional differences between the SC-constant μ and the SC-TCT μ in the distribution of CBF indicate the regional differences in the attenuation coefficient. The ratio of SC-constant μ to the SC-TCT μ was uniformly around 100% (Fig. 2, A), and the largest underestimation of CBF for the SC-constant μ as compared with the SC-TCT μ was observed in the occipital and parietal cortices and cerebellar cortex (Fig. 2, A) as reported previously.[6] This regionality might be caused by the regional differences in attenuation of the skull which are mainly caused by the regional differences in skull thickness,[28] i.e., the posterior part of the skull is thicker than other parts as commonly observed.[29]

By means of the anatomic standardization technique, slight but significant underestimation of CBF for the SC-constant μ as compared with the SC-TCT μ in all neocortical regions and overestimation in the deep cerebral white matter were observed (Fig. 2, B, C), resulting in slight reduction in contrast between gray and white matter in the SC-constant μ as compared with the SC-TCT μ (Fig. 1). This might be caused by the regional difference in the attenuation coefficient.

Since the scatter and attenuation correction with the uniform μ-map does not require the transmission scan, it can routinely be used,[6] but it is considered that there are slight but systematic differences in the distribution of CBF between the SC-constant μ and the SC-TCT μ. In addition, when the regional difference in skull thickness is large, e.g., post-craniectomy, the μ-map derived from the transmission scan should be used.[28]

Regional effects of scatter

The NoSC has been widely used for clinical routine. The regional differences between the NoSC and the SC-TCT μ in the distribution of CBF indicate regional differences in both the attenuation coefficient and scatter distribution. Since the regional difference in the attenuation coefficient was small (Fig. 2, A), the difference between the NoSC and the SC-TCT μ mainly indicates the regional difference in scatter distribution.

In the NoSC, the largest overestimation of CBF was observed in the deep cerebral white matter as compared with SC-TCT μ (Fig. 3, A), and this caused the reduction in contrast between gray and white matter in scatter uncorrected SPECT images (Fig. 1) as reported previously.[6] With the anatomic standardization technique, a significant overestimation of CBF was also observed in the pons, thalamus, putamen, hippocampal region and cingulate gyrus (Fig. 3, B). Since the scatter fraction depends on the attenuation factor,[11] scatter distribution was more in the central brain structures such as the deep cerebral white matter, pons, thalamus, putamen, hippocampal region and cingulate gyrus. The hippocampal region is of interest in the pathophysiology of Alzheimer's disease, and several investigators have detected hypoperfusion in the hippocampal region by means of SPECT.[30–32] The cingulate gyrus is also of interest in the pathophysiology of neuropsychiatric disorders, and hypoperfusion in the anterior cingulate region has been shown in depression by means of SPECT[16] but since the scatter distribution was great in these regions, the results of these reports might include the artifacts due to scatter.

In contrast to this, an underestimation was observed in all neocortical regions as reported previously.[6] With the anatomic standardization technique, the largest underestimation of CBF for the NoSC as compared with the SC-TCT μ was observed in the occipital and parietal cortices and cerebellar cortex (Fig. 3, A). This regionality might mainly be caused by the regional differences of attenuation of the skull as mentioned above.[28,29]

Comparison between scatter corrected SPECT and PET

The regional distribution of CBF was similar in SC-TCT μ and PET (Fig. 1) as reported previously,[6] but with the anatomic standardization technique, an overestimation of CBF for the SC-TCT μ was observed in the deep cerebral white matter, and an underestimation was observed in all the other regions, especially the thalamus, putamen, temporal cortex and occipital cortex (Fig. 1). These findings indicate that there are over- and underestimation of CBF for SPECT in areas with low and high CBF, respectively.[6] As reasons of this, the following factors were considered: (a) the difference between ^{123}I-IMP and $H_2{}^{15}O$ in the first-pass extraction fraction; (b) the non-linearity between CBF and radioactivity concentration in SPECT; (c) poorer spatial resolution of SPECT.

If the first-pass extraction fraction of ^{123}I-IMP was lower than that of $H_2{}^{15}O$,[2] the reduction in contrast between the areas with low and high CBF in SPECT would be caused. In the present study, the SPECT scan was performed from 20 to 40 min after intravenous infusion of ^{123}I-IMP. The ^{123}I-IMP SPECT image obtained by integration for this time interval has been shown to be similar to CBF image obtained by the kinetic analysis with ^{123}I-IMP,[2] but the relation between radioactivity integrated for this time interval and CBF was not linear.[3] This might cause the reduction in contrast between the areas with low and high CBF. As reported previously,[6] poorer spatial resolution of SPECT would cause the reduction in contrast due to an increase in the partial volume effect.

CONCLUSION

In the NoSC, a significant overestimation of CBF was observed in the deep cerebral white matter, pons, thalamus, putamen, hippocampal region and cingulate gyrus as compared with the SC-TCT μ. A significant underestimation was observed in all neocortical regions, especially in the occipital and parietal lobes, and the cerebellar cortex. The regional distribution of CBF between SC-constant μ and SC-TCT μ was in good agreement, however slight but systematic differences in the distribution of CBF were observed. The regional distribution of CBF obtained with the SC-TCT μ was similar to that obtained by PET. The scatter correction is needed for the assessment of CBF with SPECT, and both the TDCS methods which employ the constant μ-map and the μ-map derived from the transmission scan can be used for scatter correction of SPECT.

ACKNOWLEDGMENTS

The assistance of the members in Akita Research Institute of Brain and Blood Vessels involved in the SPECT and PET experiments is also gratefully acknowledged.

REFERENCES

1. Winchell HS, Baldwin RM, Lin TH. Development of I-123-labeled amines for brain studies: Localization of I-123 iodophenylalkyl amines in rat brain. *J Nucl Med* 21: 940–946, 1980.
2. Ito H, Iida H, Bloomfield PM, Murakami M, Inugami A, Kanno I, et al. Rapid calculation of regional cerebral blood flow and distribution volume using iodine-123-iodoamphetamine and dynamic SPECT. *J Nucl Med* 36: 531–536, 1995.
3. Iida H, Itoh H, Nakazawa M, Hatazawa J, Nishimura H, Onishi Y, et al. Quantitative mapping of regional cerebral blood flow using iodine-123-IMP and SPECT. *J Nucl Med* 35: 2019–2030, 1994.
4. Ito H, Koyama M, Goto R, Kawashima R, Ono S, Atsumi H, et al. Cerebral blood flow measurement with iodine-123-IMP SPECT, calibrated standard input function and venous blood sampling. *J Nucl Med* 36: 2339–2342, 1995.

5. Ito H, Ishii K, Atsumi H, Inukai Y, Abe S, Sato M, et al. Error analysis of autoradiography method for measurement of cerebral blood flow by ^{123}I-IMP brain SPECT: A comparison study with table look-up method and microsphere model method. *Ann Nucl Med* 9: 185–190, 1995.
6. Iida H, Narita Y, Kado H, Kashikura A, Sugawara S, Shoji Y, et al. Effects of scatter and attenuation correction on quantitative assessment of regional cerebral blood flow with SPECT. *J Nucl Med* 39: 181–189, 1998.
7. Axelsson B, Msaki P, Israelsson A. Subtraction of Compton-scattered photons in single-photon emission computerized tomography. *J Nucl Med* 25: 490–494, 1984.
8. Ogawa K, Harata Y, Ichihara T, Kubo A, Hashimoto S. A practical method for position-dependent Compton-scatter correction in single photon emission CT. *IEEE Trans Med Imag* 10: 408–412, 1991.
9. Ichihara T, Ogawa K, Motomura N, Kubo A, Hashimoto S. Compton scatter compensation using the triple-energy window method for single- and dual-isotope SPECT. *J Nucl Med* 34: 2216–2221, 1993.
10. Ogawa K, Ichihara T, Kubo A. Accurate scatter correction in single photon emission CT. *Ann Nucl Med* 7: 145–150, 1994.
11. Meikle SR, Hutton BF, Bailey DL. A transmission-dependent method for scatter correction in SPECT. *J Nucl Med* 35: 360–367, 1994.
12. Ljungberg M, King MA, Hademenos GJ, Strand SE. Comparison of four scatter correction methods using Monte Carlo simulated source distributions. *J Nucl Med* 35: 143–151, 1994.
13. Buvat I, Rodriguez-Villafuerte M, Todd-Pokropek A, Benali H, Di Paola R. Comparative assessment of nine scatter correction methods based on spectral analysis using Monte Carlo simulations. *J Nucl Med* 36: 1476–1488, 1995.
14. Narita Y, Eberl S, Iida H, Hutton BF, Braun M, Nakamura T, et al. Monte Carlo and experimental evaluation of accuracy and noise properties of two scatter correction methods for SPECT. *Phys Med Biol* 41: 2481–2496, 1996.
15. Fox PT, Mintun MA, Reiman EM, Raichle ME. Enhanced detection of focal brain responses using intersubject averaging and change-distribution analysis of subtracted PET images. *J Cereb Blood Flow Metab* 8: 642–653, 1988.
16. Ito H, Kawashima R, Awata S, Ono S, Sato K, Goto R, et al. Hypoperfusion in the limbic system and prefrontal cortex in depression: SPECT with anatomic standardization technique. *J Nucl Med* 37: 410–414, 1996.
17. Minoshima S, Berger KL, Lee KS, Mintun MA. An automated method for rotational correction and centering of three-dimensional functional brain images. *J Nucl Med* 33: 1579–1585, 1992.
18. Minoshima S, Koeppe RA, Mintun MA, Berger KL, Taylor SF, Frey KA, et al. Automated detection of the intercommissural line for stereotactic localization of functional brain images. *J Nucl Med* 34: 322–329, 1993.
19. Minoshima S, Koeppe RA, Frey KA, Kuhl DE. Anatomic standardization: Linear scaling and nonlinear warping of functional brain images. *J Nucl Med* 35: 1528–1537, 1994.
20. Minoshima S, Koeppe RA, Frey KA, Ishihara M, Kuhl DE. Stereotactic PET atlas of the human brain: aid for visual interpretation of functional brain images. *J Nucl Med* 35: 949–954, 1994.
21. Vander Borght T, Minoshima S, Giordani B, Foster NL, Frey KA, Berent S, et al. Cerebral metabolic differences in Parkinson's and Alzheimer's diseases matched for dementia severity. *J Nucl Med* 38: 797–802, 1997.
22. Hudson HM, Larkin RS. Accelerated image reconstruction using ordered subsets of projection data. *IEEE Trans Med Imag* MI-13: 601–609, 1994.
23. Iida H, Miura S, Kanno I, Ogawa T, Uemura K. A new PET camera for noninvasive quantitation of physiological functional parametric images: Headtome-V-dual. *In*: Myers R, Cunningham Y, Bailey D, Jones T, eds. *Quantification of Brain Function Using PET*. San Diego: Academic Press, pp. 57–61, 1996.
24. Iida H, Kanno I, Takahashi A, Miura S, Murakami M, Takahashi K, et al. Measurement of absolute myocardial blood flow with $H_2{}^{15}O$ and dynamic positron-emission tomography. Strategy for quantification in relation to the partial-volume effect. *Circulation* 78: 104–115, 1988.
25. Iida H, Rhodes CG, de Silva R, Araujo LI, Bloomfield PM, Lammertsma AA, et al. Use of the left ventricular time-activity curve as a noninvasive input function in dynamic oxygen-15-water positron emission tomography. *J Nucl Med* 33: 1669–1677, 1992.
26. Raichle ME, Martin WR, Herscovitch P, Mintun MA, Markham J. Brain blood flow measured with intravenous $H_2{}^{15}O$. II. Implementation and validation. *J Nucl Med* 24: 790–798, 1983.
27. Kanno I, Iida H, Miura S, Murakami M, Takahashi K, Sasaki H, et al. A system for cerebral blood flow measurement using an $H_2{}^{15}O$ autoradiographic method and positron emission tomography. *J Cereb Blood Flow Metab* 7: 143–153, 1987.
28. Stodilka RZ, Kemp BJ, Prato FS, Nicholson RL. Importance of bone attenuation in brain SPECT quantification. *J Nucl Med* 39: 190–197, 1998.
29. Law SK. Thickness and resistivity variations over the upper surface of the human skull. *Brain Topogr* 6: 99–109, 1993.
30. Waldemar G, Christiansen P, Larsson HB, Hogh P, Laursen H, Lassen NA, et al. White matter magnetic resonance hyperintensities in dementia of the Alzheimer type: Morphological and regional cerebral blood flow correlates. *J Neurol Neurosurg Psychiatry* 57: 1458–1465, 1994.
31. Ohnishi T, Hoshi H, Nagamachi S, Jinnouchi S, Flores LG II, Futami S, et al. High-resolution SPECT to assess hippocampal perfusion in neuropsychiatric diseases. *J Nucl Med* 36: 1163–1169, 1995.
32. Lehtovirta M, Soininen H, Laakso MP, Partanen K, Helisalmi S, Mannermaa A, et al. SPECT and MRI analysis in Alzheimer's disease: Relation to apolipoprotein E epsilon 4 allele. *J Neurol Neurosurg Psychiatry* 60: 644–649, 1996.